REPORT DOCUMENTATION PAGE

Form Approved OMB NO. 0704-0188

1. REPORT DATE (DD-MM-YYYY)	2. REPORT TYPE	3. DATES COVERED (From - To)
	New Reprint	-

4. TITLE AND SUBTITLE

Chirped fiber Brillouin frequency-domain distributed sensing

5a. CONTRACT NUMBER	5b. GRANT NUMBER	5c. PROGRAM ELEMENT NUMBER
W911NF-12-1-0602		

6. AUTHORS

Peter D. Dragic, Anthony Mangognia, John Ballato

5d. PROJECT NUMBER	5e. TASK NUMBER	5f. WORK UNIT NUMBER

7. PERFORMING ORGANIZATION NAMES AND ADDRESSES

University of Illinois - Urbana
1901 S. First Street, Suite A

Champaign, IL 61820 -7406

8. PERFORMING ORGANIZATION REPORT NUMBER

9. SPONSORING/MONITORING AGENCY NAME(S) AND ADDRESS (ES)

U.S. Army Research Office
P.O. Box 12211
Research Triangle Park, NC 27709-2211

10. SPONSOR/MONITOR'S ACRONYM(S)
ARO

11. SPONSOR/MONITOR'S REPORT NUMBER(S)
62081-PH-HEL.13

12. DISTRIBUTION AVAILIBILITY STATEMENT

Approved for public release; distribution is unlimited.

13. SUPPLEMENTARY NOTES

The views, opinions and/or findings contained in this report are those of the author(s) and should not contrued as an official Department of the Army position, policy or decision, unless so designated by other documentation.

14. ABSTRACT

A frequency-domain distributed temperature/strain sensor based on a longitudinally graded optical fiber (LGF) is proposed and evaluated. In an LGF, the Brillouin scattering frequency, ? B , changes (i.e., is chirped) lengthwise monotonically and thus every position along the fiber has a unique ? B . Any change locally (at some position) in the fiber environment will result in a measurable change in the shape of the Brillouin gain spectrum (BGS) near the frequency component mapped to that position. This is demonstrated via measurements and modeling for an LGF with local heating. The LGF is one with 210?32MHz Brillouin frequency gradient over 16.7 m, with 1.1 and 1.7 m

15. SUBJECT TERMS

Brillouin scattering; optical fiber sensors; distributed sensing; frequency domain

16. SECURITY CLASSIFICATION OF:			17. LIMITATION OF ABSTRACT	15. NUMBER OF PAGES	19a. NAME OF RESPONSIBLE PERSON
a. REPORT	b. ABSTRACT	c. THIS PAGE			Peter Dragic
UU	UU	UU	UU		19b. TELEPHONE NUMBER 217-333-8399

Report Title

Chirped fiber Brillouin frequency-domain distributed sensing

ABSTRACT

A frequency-domain distributed temperature/strain sensor based on a longitudinally graded optical fiber (LGF) is proposed and evaluated. In an LGF, the Brillouin scattering frequency, ? B , changes (i.e., is chirped) lengthwise monotonically and thus every position along the fiber has a unique ? B . Any change locally (at some position) in the fiber environment will result in a measurable change in the shape of the Brillouin gain spectrum (BGS) near the frequency component mapped to that position. This is demonstrated via measurements and modeling for an LGF with local heating. The LGF is one with ?100??MHz Brillouin frequency gradient over 16.7 m, with 1.1 and 1.7 m segments heated up to 40 K above ambient. A measurement of the BGS can enable the determination of a thermal (or strain) distribution along a sensor fiber, thus rendering the system one that is in the frequency domain. A sensitivity analysis is also presented for both coherent and pump-probe BGS measurement schemes. The modeling results suggest that the frequency-domain systems based on fibers with a chirped Brillouin frequency are highly suited as inexpensive event sensors (alarms) and have the potential to reach submeter position determination with sub-1-K temperature accuracies at >1??kHz sampling rates. Limitations to the technique are discussed.

REPORT DOCUMENTATION PAGE (SF298)
(Continuation Sheet)

Continuation for Block 13

ARO Report Number 62081.13-PH-HEL
Chirped fiber Brillouin frequency-domain distribu...

Block 13: Supplementary Note

Approved for public release; distribution is unlimited.

Optical Engineering

SPIEDigitalLibrary.org/oe

Chirped fiber Brillouin frequency-domain distributed sensing

Peter D. Dragic
Anthony Mangognia
John Ballato

Chirped fiber Brillouin frequency-domain distributed sensing

Peter D. Dragic,[a,*] Anthony Mangognia,[a] and John Ballato[b]
[a]University of Illinois at Urbana-Champaign, Department of Electrical and Computer Engineering, 1406 W. Green Street, Urbana, Illinois 61822
[b]Clemson University, Center for Optical Materials Science and Engineering Technologies, Department of Materials Science and Engineering, 91 Technology Drive, Anderson, South Carolina 29625

Abstract. A frequency-domain distributed temperature/strain sensor based on a longitudinally graded optical fiber (LGF) is proposed and evaluated. In an LGF, the Brillouin scattering frequency, ν_B, changes (i.e., is chirped) lengthwise monotonically and thus every position along the fiber has a unique ν_B. Any change locally (at some position) in the fiber environment will result in a measurable change in the shape of the Brillouin gain spectrum (BGS) near the frequency component mapped to that position. This is demonstrated via measurements and modeling for an LGF with local heating. The LGF is one with ~100 MHz Brillouin frequency gradient over 16.7 m, with 1.1 and 1.7 m segments heated up to 40 K above ambient. A measurement of the BGS can enable the determination of a thermal (or strain) distribution along a sensor fiber, thus rendering the system one that is in the frequency domain. A sensitivity analysis is also presented for both coherent and pump-probe BGS measurement schemes. The modeling results suggest that the frequency-domain systems based on fibers with a chirped Brillouin frequency are highly suited as inexpensive event sensors (alarms) and have the potential to reach submeter position determination with sub-1-K temperature accuracies at >1 kHz sampling rates. Limitations to the technique are discussed. [DOI: 10.1117/1.OE.53.5.056117]

Keywords: Brillouin scattering; optical fiber sensors; distributed sensing; frequency domain.

Paper 140195P received Feb. 1, 2014; revised manuscript received Apr. 17, 2014; accepted for publication May 2, 2014; published online May 28, 2014.

1 Introduction

The Brillouin scattering frequency, ν_B, is related to the optical wavelength, λ_o, and the acoustic velocity, V, by $\nu_B = 2Vn_{\text{mode}}/\lambda_o$. It is well known that both the acoustic velocity and the refractive index of a glass usually are functions of its thermomechanical environment; i.e., temperature and any applied stress or strain to the material. The word "usually" is used as a qualifier because it is possible to realize multicomponent materials of which physical properties, such as the refractive index, are immune to temperature or strain/stress.[1–4] However, in conventional pure silica or GeO_2-doped silica core optical fibers, the Brillouin scattering frequency is dependent on both the temperature and strain, with the usual dependence being an increasing frequency with increasing temperature or strain.[5]

Since the temperature and strain dependencies of the Brillouin frequency (typically ~1.2 MHz/K[6] and 500 MHz/%,[7] respectively, near 1550 nm for conventional fiber[5]) are not insignificant, it is natural that this phenomenon has been adapted for use in distributed sensor technologies,[8–11] with very impressive results. High-sensitivity and resolution measurement schemes and configurations have been demonstrated,[12–20] and a commercial market exists for such distributed sensing systems. Resolution is defined in this context to be the ability to resolve two events that are in close proximity to each other, or alternatively, to resolve a certain temperature or strain change within a given range in the sensor fiber. Sensitivity is, then, the minimum detectable change in temperature or strain. In recent years, there has been a significant push toward the achievement of remarkable spatial and thermal/strain resolutions (reviews may be found in Ref. 21 and 22). However, in many applications, sub-centimeter measurement resolutions (or rather spatial resolutions of order $\ll 10^{-4}$ of the total sensor length) are not necessary, and instead robustness, simplicity, fast sampling times, and low cost are primary concerns. Examples of such cases might be fire detection in buildings, tunnels, etc.,[23] leak detection,[24] machines,[25] and perimeter security (or intrusion sensing),[26] to name a few.

Such Brillouin systems are labeled as "distributed" because they are capable of correlating a lengthwise thermal or strain distribution in a deployed sensor fiber. In a way fully analogous to a light detection and ranging (LIDAR) system, time-domain measurements are achieved by launching a pulse of narrow linewidth light into a fiber and receiving time-gated returns corresponding to Brillouin scattering or gain from known positions along the fiber. Thus, these systems are commonly referred to as Brillouin optical time-domain reflectometry or analyzer systems,[14,27] respectively. Some work has been done in the frequency domain (i.e., Brillouin frequency-domain systems[28,29] as well as non-Brillouin configurations[30]), with promising and impressive results, but Brillouin frequency-domain systems are far rarer than their time-domain counterparts.

Continuing with the LIDAR analogy, typical atmospheric systems are sometimes employed to measure weather conditions, such as temperature or wind speeds.[31] They rely on atmospheric scattering phenomena, such as Rayleigh

*Address all correspondence to: Peter D. Dragic, E-mail: p-dragic@illinois.edu

scattering[32] or resonance fluorescence,[33] as a probe from which atmospheric attributes may be determined. With a LIDAR system, one is limited to designing optical systems based on the whims of Mother Nature. One would be hard-pressed to design and implement a custom atmospheric column that would lead to a more sensitive probe of the environment.

While many systems utilize conventional optical fiber in distributed sensing applications, this is tantamount to submitting to Mother Nature's whim, and there is nothing necessarily precluding the design of a more ideal optical fiber that can serve to improve the sensitivity or to enhance the capabilities of a Brillouin-based distributed sensor. For example, acoustic waveguide designs can be implemented that give rise to multiple Brillouin frequencies being present in a single fiber such that simultaneous measurements of temperature or strain can be made[34,35] with a single sensor fiber. More recently, it was proposed that designer materials can be engineered for which Brillouin frequencies are immune to temperature[36] or strain.[37] One may even envision the possibility of a material with enhanced Brillouin gain.

Also recently, a novel way of fabricating a fiber, for which material composition is lengthwise graded (longitudinally graded fiber, or LGF), was proposed and experimentally demonstrated.[38] Briefly, a core slug is drilled from a graded-index (core) fiber preform, sleeved, and then drawn into an LGF. One purpose of such a fiber is to broaden the Brillouin spectrum in order to suppress stimulated Brillouin scattering (SBS), among a number of other applications.[38] While SBS suppression appears to be a highly promising application for this technology, another very interesting application is distributed sensing in the frequency domain. In a traditional time-domain system, the Brillouin gain spectrum (BGS) of a sensor fiber is typically uniform along a length of fiber. Changes in the value of ν_B lead to measurements of the local temperature or strain, and thus intuitively it can be reasoned that the narrower the BGS, the more sensitive the measurement. In an LGF, however, since ν_B [or more accurately $\nu_B(z)$] is changing (i.e., chirped) lengthwise monotonically, then every position on the fiber has a unique ν_B with which it is associated. If such a fiber is deployed in a sensor network, then, any change locally in the fiber environment will result in a measurable change in the measured BGS.

More specifically, the measured BGS will be broadened from the intrinsic (nonLGF) BGS, which is a Lorentzian function, due to $\nu_B(z)$, which also includes any associated thermal or strain distribution along the fiber. The reverse, then, is also true: a measurement of the BGS gives rise to a measurement of $\nu_B(z)$. If this distribution is known for the "unperturbed" (e.g., room temperature and zero strain) fiber, then the change in $\nu_B(z)$ from its unperturbed state gives rise to a distributed measurement of temperature/strain. This is interesting since now a continuous wave (CW) measurement of the BGS, rather than time-gated returns of a pulse, affords a measurement of the environmental distribution of the fiber, that is, a frequency-domain system.

In this paper, the feasibility of such a frequency-domain Brillouin-based distributed sensor is investigated. The paper has three parts. First, the BGS of an LGF is modeled, including the effect of a local environmental event. Thermal effects are utilized as a convenient example, where it is shown that a measureable change in the BGS is the result of a change in lengthwise temperature distribution. The corollary case for strain or simultaneously both temperature and strain is straightforward although not exemplified herein. Second, utilizing the LGF optical fiber from Evert et al.,[38] the model and the measurable change in the BGS are validated experimentally. Finally, a sensitivity analysis is presented to estimate the signal-to-noise ratio (SNR) and resolution of such a system. Both pump-probe and coherent-detection schemes for measuring the BGS are investigated. Modeling results suggest that the frequency-domain systems based on fibers with a chirped Brillouin frequency have a significant potential for event sensors (such as alarm systems) with rapid measurement times.

2 Modeling the Spectrum

It is well known that the BGS of a uniform optical fiber is expressed as a Lorentzian function of the frequency ν using the form

$$g_B(\nu) = \frac{g_{B0}}{1 + \left(\frac{\nu - \nu_B}{\Delta\nu_B/2}\right)^2}, \tag{1}$$

where ν_B is the central frequency and $\Delta\nu_B$ is the Brillouin spectral width (full width at half maximum). The central frequency is determined from a combination of the Bragg condition and the acoustic velocity, V_a, via $\nu_B = 2n_m V_a/\lambda_o$ with λ_o being the vacuum optical wavelength and n_m being the effective modal index as noted in the Introduction. In Eq. (1), g_{B0} is the peak Brillouin gain coefficient, which is a function of V_a, $\Delta\nu_B$, n, mass density, and the photoelastic constant (Pockels' coefficient) of the material through which the light is propagating.

For LGFs, the central frequency becomes a function of distance, i.e., $\nu_B \rightarrow \nu_B(z)$. For fibers with a lengthwise uniform refractive index difference, this means that $V_a \rightarrow V_a(z)$ due to the compositional variation. In addition to the acoustic velocity, since $\Delta\nu_B$ is proportional to the square of the central frequency [Eq. (1)], and the central frequency is a function of distance, $\Delta\nu_B$ is also a function of position along the fiber, z. Hence, g_{B0} also is a function of z courtesy of $V_a(z)$ and $\Delta\nu_B(z)$.

The simplest configuration of the BGS is a linear dependence of central frequency with distance, z, along the fiber such that $\nu_B \rightarrow \nu_B - Cz$, where C is a constant. In this case, the Brillouin spectrum is spread approximately uniformly across all available acoustic frequencies, thereby flattening the effective BGS. In order to compute the measured BGS from such a structure, one assumes, to first order, that only the central frequency is z-dependent (i.e., the z-dependence of the other parameters such as the photoelastic constant and Brillouin spectral width is negligible) and that the fiber is optically lossless. Then, with the assumption that Eq. (1) represents the local BGS in the LGF, integration over all z (for a fiber of length L) is performed in order to obtain for the measured BGS that

$$g_B(\nu) = \frac{\Delta\nu_B}{2LC}\left\{\arctan\left[2\frac{(\nu - \nu_B) + CL}{\Delta\nu_B}\right] - \arctan\left[2\frac{(\nu - \nu_B)}{\Delta\nu_B}\right]\right\}. \tag{2}$$

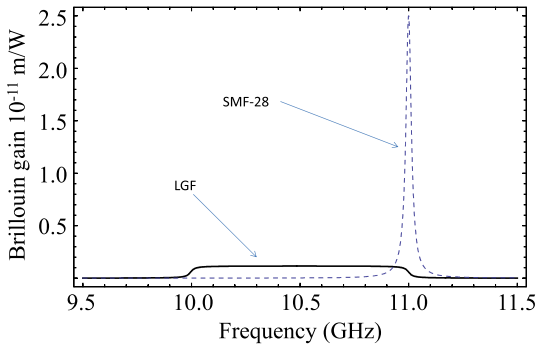

Fig. 1 Brillouin gain spectra for a conventional single mode fiber (SMF-28) and that of the longitudinally graded optical fiber (LGF).

Next, assumed here is a starting central frequency (i.e., at one end) of 11 GHz and intrinsic Brillouin spectral width of 30 MHz to approximately match the measured characteristics of the SMF-28 fiber[39] that is used for comparison. The fiber length, L, is assumed to be 1000 m with the additional assumption that the fiber has a linearly distributed total frequency breadth of 1 GHz (a path toward such a fiber using GeO_2 and F co-doping is outlined in Evert et al.[38]), then $C = 1$ MHz/m. It is noted that the value of C is a design parameter that can be controlled in the fiber fabrication process. Equation (2) has been normalized so that the total integrated Brillouin gain with respect to ν is conserved between the uniform and longitudinally graded fibers[38,40] and that the maximum Brillouin gain in a uniform fiber is about 2.5×10^{-11} m/W.[39] Using these values in Eq. (2), Fig. 1 computes the BGS for a lengthwise un-chirped and chirped Brillouin frequencies. A clear disadvantage to the use of the LGF in the Brillouin sensing application is the considerable reduction in the Brillouin gain and the "specialty" nature introducing a level of greater fabrication complexity, at least currently, over conventional telecom-grade fiber. However, it is expected that as LGF technology matures, fabrication of such fibers will become much more routine.

In the LGF, a change in temperature or strain at some position along the fiber will result in a change in the local ν_B. Usually, as with GeO_2-doped silica fibers, an increase in strain or temperature will cause an increase in ν_B. What, then, happens in either of these two cases is intuitive: in some region of the BGS, corresponding to some position along the fiber, ν_B will shift to a larger value, leaving a spectral dip and a peak at higher frequency where the shifted spectral slice contributes to spectral slices from other positions on the fiber.

Modeling the system constitutes replacing the $\nu_B(z) = \nu_B - Cz$ with a new, more appropriate function. For the example, presented here, it will be assumed that any local heating event along the sensor fiber will be Gaussian distributed with some linewidth (spatial extent). Therefore, the new lengthwise frequency distribution in the fiber can be written as

$$\nu_B(z) = \nu_B - \left\{ Cz - \Delta T C_T \exp\left[-\left(\frac{z - L'}{\Delta L} \right)^2 \right] \right\}, \tag{3}$$

where ΔT is the change in temperature, C_T is the thermal coefficient of the Brillouin frequency shift (MHz/K), and ΔL limits the range over which the fiber is being heated. Equation (3) is substituted into Eq. (1) and numerically integrated as with the case of the simple linear frequency distribution. As an example, retaining the values previously stated and assuming that $\Delta L = 10$ m, $C_T = 1.1$ MHz/K and $L' = 250$ m (position of the heating incident), Fig. 2 plots the BGS for $\Delta T = 0$, 10, and 30 K demonstrating how its shape and distribution changes with a local heating event. While the example presented here is that of heating, similar results are obtained for the strain where Eq. (3) would change, so that $\Delta T \to \varepsilon$ (strain) and $C_T \to C_\varepsilon$ (strain coefficient in units of MHz/elongation).

First, changing the position of the environmental event simply shifts the position of the spectral "anomaly." This is illustrated in Fig. 2(a), in which the BGS is recalculated for the $\Delta T = 30$ K case, but with L' now equal to 750 m. Second, since the intrinsic Brillouin spectrum has a width of about 30 MHz locally along the fiber, a reduction in ΔL causes the amplitude or strength of the change in the BGS to reduce since a narrower sliver of spectrum is being shifted. In order to demonstrate this, the calculation shown in Fig. 2(b) is repeated for $\Delta L = 2$ m, and the result is shown in Fig. 3. Thus, it is clear that as the spatial resolution (or the distance over which the event takes place) is increased, the sensitivity of the measurement of the fiber environment is reduced. A sensitivity analysis is presented in a subsequent section.

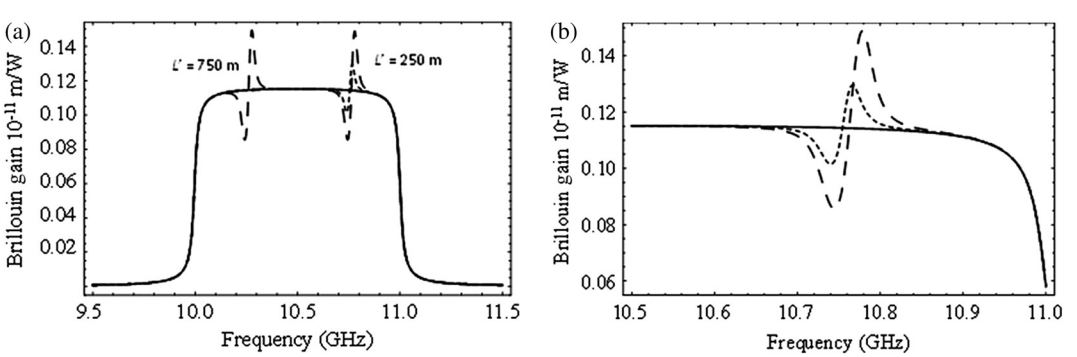

Fig. 2 (a) Brillouin gain spectrum for the example for $\Delta T = 0$, 10, and 30 K, (b) expanded view in the vicinity of the thermal activity region ("anomaly"). The amplitude of the change in BGS increases with increasing temperature. Changing L' simply shifts the location of the spectral "anomaly" as illustrated with the $\Delta T = 30$ K calculation repeated for 750 m [shown in (a)].

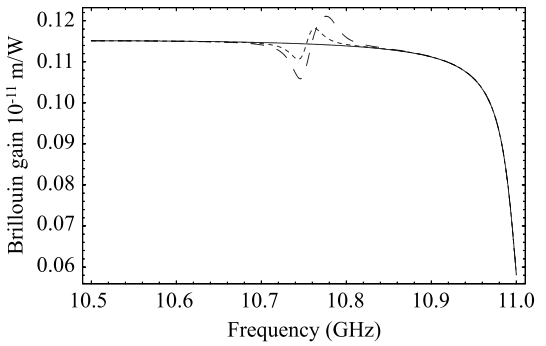

Fig. 3 Brillouin gain spectrum for the example for $\Delta T = 0$, 10, and 30 K and ΔL now equal to 2 m.

3 Validation of the Model and Proof-of-Concept

The LGF fiber described previously in Evert et al.[38] is utilized in the following set of measurements and modeling calculations. This fiber, due to its acoustically guiding nature,[41] exhibits multiple acoustic modes in its BGS. However, the higher order acoustic modes will be neglected, and a focus will be made on the fundamental (lowest frequency) acoustic mode since it is also the strongest. The measurement apparatus employed is identical to that in Dragic,[42] and therefore it will not be described in detail here. However, in short, it is a heterodyne system wherein a pump signal is launched into a test fiber, generating spontaneous Brillouin scattering. Said signal is optically amplified and mixed with the pump using a fast lightwave receiver, and the resulting beat spectrum is recorded with an electrical spectrum analyzer. The measured BGS for the ($F + GeO_2$ co-doped silica core) LGF of this study is shown in Fig. 4. The spectrum is not flat, and thus the lengthwise distribution of Brillouin frequencies is not linear. A fit was, therefore, performed to determine an approximate distribution. The distribution that gave the best fit to the BGS was determined to be

$$\nu_B(z) = \nu_B - (Cz + C'z^{1.45}), \tag{4}$$

where $\nu_B = 10.8985$ GHz, $C = 0.93$ MHz/m, $C' = 1.45$ MHz/m$^{1.45}$, and $\Delta\nu_B = 39.5$ MHz. Substituting Eq. (4) into Eq. (1) and integrating over z gives the simulated BGS provided in Fig. 4 (as the dashed line). There is excellent agreement between the measured and modeled BGS,

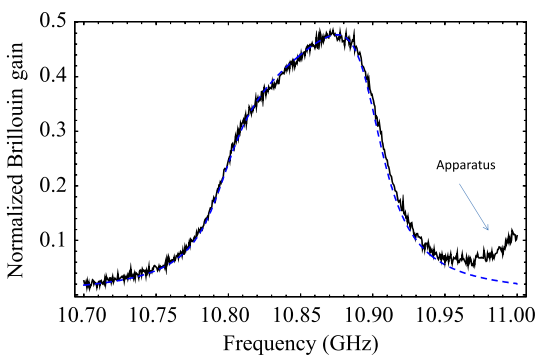

Fig. 4 Brillouin gain spectrum of the fundamental acoustic mode of the LGF of this study (solid line). The modeling fit to the data is also shown (dashed line).The total fiber length is 16.7 m.

affording considerable confidence in the results and analysis that follows.

Conceptually, heating and straining the fiber give rise to essentially identical changes to the BGS. However, since heating a small segment of the 16.7-m fiber was far easier to implement than applying strain, heating experiments were performed and treated here. Heating a fiber was accomplished by placing a segment of test fiber into a well-controlled heated water bath. This type of thermal distribution is more like a uniform function over some range ΔL. Thus, the thermal distribution denoted in Eq. (3) is modified from possessing a simple Gaussian function to possessing a super-Gaussian function. Therefore, the modified final distribution of frequencies for the LGF is given by

$$\nu_B(z) = \nu_B - \left\{ Cz + C'z^{1.45} - \Delta T C_T \exp\left[-\left(\frac{z - L'}{\Delta L} \right)^{2M} \right] \right\}. \tag{5}$$

As stated before, Eq. (5) is substituted into Eq. (1) and the result is integrated over z to yield a calculation of the BGS as a function of temperature. For the first example, $L' = 9.7$ m and $\Delta L = 1.13$ m, with the Brillouin spectra calculated and measured for $\Delta T = 5$, 10, 20, and 40 K. C_T was found to be 1.11 MHz/K for the LGF.[5,34] Figures 5(a) and 5(b) show the modeled (using $M = 20$ to simulate the uniform heating of a segment of fiber) and measured normalized BGS for the various temperatures, respectively. The normalization procedure was to assume the Brillouin gain of an unchirped (uniform) fiber with the same $\Delta\nu_B$ is unity. Figures 6(a) and 6(b) provide the results of a slightly modified set of conditions where $L' = 9.9$ m and $\Delta L = 1.70$ m, $\Delta T = 5$, 15, 25, and 45 K. As seen, there is excellent agreement between the measured and modeled BGS. As described, changing L' only serves to shift the position of the dip ("anomaly") in the spectrum; however, since the spectral breadth of the proof-of-concept LGF used in this study was only about 100 MHz, performing such an investigation would add little to the present analysis.

In summary, it has been shown that by heating (or, in theory, straining) a small segment of LGF (chirped fiber) at some position, a measurable change in the BGS can be realized. As such, in principle, the reverse process is then also possible, in that if a BGS of an LGF in an unknown environment is measured, comparing this to the unheated (unstrained) spectrum discloses the thermal (or strain) distribution. While the method used to measure the BGS in the present analysis is optimized neither for cost nor sensitivity and the available length of a fiber was limited, it provides for a reasonable proof-of-concept. Depending on the configuration, a considerable improvement in sensitivity can be achieved. This is described in more detail in Sec. 5.

4 Limitations to Scheme

4.1 *Uniqueness of the Brillouin Gain Spectrum*

For any known thermal or strain distribution along the LGF, the BGS can be calculated. This assumes that the unperturbed BGS for the fiber is known. However, more complex situations, such as the simultaneous presence of multiple, randomly distributed heating or strain events, pose a problem when a unique Brillouin spectrum from an LGF is needed to

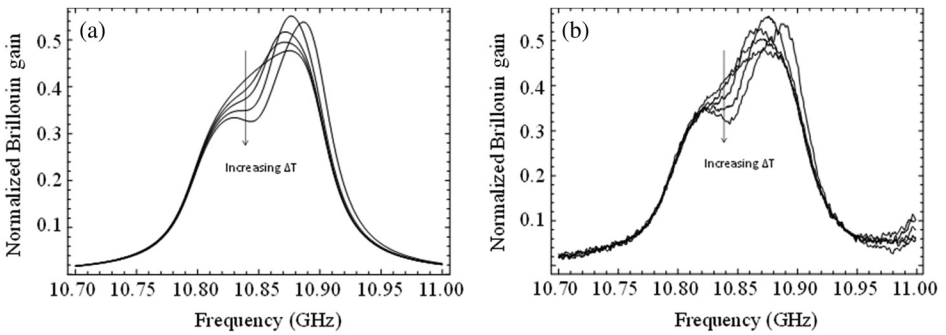

Fig. 5 (a) Modeled BGS of the LGF at $\Delta T = 0$, 5, 10, 20, 40 K and $L' = 9.7$ m and $\Delta L = 1.13$ m, (b) measured BGS for the same thermal conditions.

identify the locations of such multiple events. Although such a result may be difficult to achieve; in practice, it is possible that two or more unique perturbation (heating or strain) distributions influence the BGS in such a way that results in identical SBS spectra. This can introduce considerable uncertainty when the proposed sensing technique is used for applications where precise identification of the location of an "event" must be determined. This will be illustrated next through the presentation of a simple example.

Consider the case of two anomalous heating events occurring at time $t = t_0$ but located at different positions along a single LGF (i.e., one at a lower and the other at a higher frequency spectral "position"), as shown in Fig. 7 (solid thick line). The reader is reminded that a spectral position on the unperturbed BGS corresponds to a unique position along the LGF. Continued heating for $t > t_0$ will cause the spectral perturbations to shift in frequency (along the direction of the black arrows) until the temperature reaches equilibrium or as heating continues. In such a case, the perturbation from the heating event at the lower frequency position along the LGF can eventually shift in frequency until it reaches the same position in the frequency domain as the second heating event. Thus, the spectral slice from the first heating event can shift and "fill-in" the hole representing the second heating event (as shown by the thick, dashed line). The resulting BGS may, then, have the appearance of being caused by a single, much hotter thermal event with a larger single shift in the BGS, rather than one resulting from two or more independent and weaker events. In such cases, therefore, multiple heating events may appear as fewer heating events, making it difficult to identify the location and the extent of the various perturbations.

Alternatively, the nonuniqueness of the BGS may introduce uncertainty in the actual temperature or strain distribution, even if the positions of the events are known. This can be the case if multiple identical events become spectrally nonsequential. For example, simultaneous, identical events may result from various amounts of temperature or strain. In which case, it is possible that some "hotter" or higher strain events may move past others within the frequency domain, making it difficult to associate the specific magnitude of an event with its location along the LGF. Referring to Fig. 8 (for the example of fiber heating), the example BGS clearly illustrates that at least two heating events have taken place; however, it is not clear which of the two is at the higher frequency.

4.2 *Continuous Monitoring of the Brillouin Gain Spectrum*

It is worth noting that the change in frequency due to the first event described in the first example above would need to be a singular value in order for the overlapped heating (or strain) events to render the BGS wholly ambiguous. For systems or applications where the possibility of only a few anomalous thermal or strain events exists, this scenario is unlikely. However, for a complex distribution where perturbations occur on a small length scale and are very close together, this becomes a more serious problem. Therefore, as mentioned in the Introduction, this type of sensing system is best suited for inexpensive and rapid sense alarms that look for significant "events" rather than small drifts in temperature or strain. However, in order to resolve the problem of identifying multiple identical overlapping heating events, the fiber BGS can be monitored continuously and compared

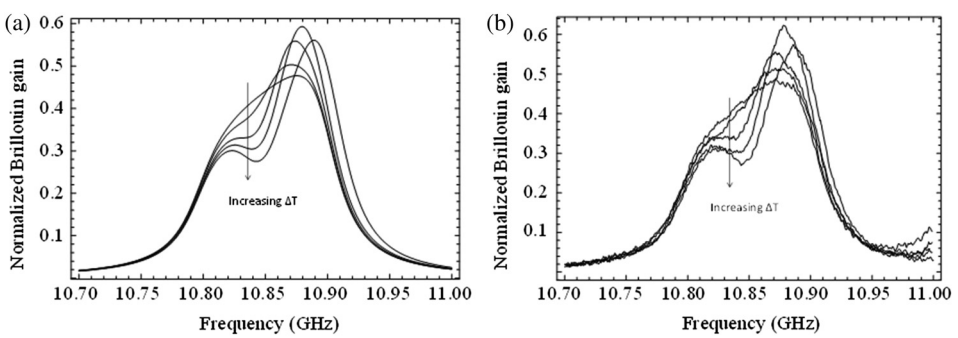

Fig. 6 (a) Modeled BGS of the LGF at $\Delta T = 0, 5, 15, 25, 45$ K and $L' = 9.9$ m and $\Delta L = 1.70$ m, (b) measured BGS for the same thermal conditions.

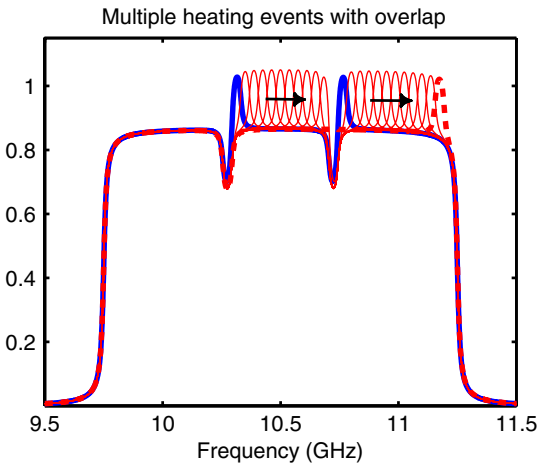

Fig. 7 Multiple heating, or strain, events may not be identifiable if the resulting perturbations to the SBS spectrum are identical and overlap. In this case, two heating events appear in the SBS spectrum, shown with the thick solid line. As temperature increases, the perturbations on the SBS spectrum shift with time, as shown by the thin solid lines. Eventually, the perturbations can overlap, resulting in the appearance of a single large temperature event, as shown by the dashed line.

with those at previous times. This enables the observation and tracking of the perturbations within the SBS spectrum as they shift in frequency with time before they overlap. Referring back to Fig. 7, with just a few measurements of the BGS just after time $t = t_0$, but on a time scale faster than that of the thermal perturbation, the location and positions of the perturbation become clear, despite the eventual overlapping spectra. Furthermore, the same is true of the example in Fig. 8; measurements of the BGS as a function of time can disclose which location along the fiber has undergone a more significant perturbation. A discussion of the rapidity, with which a measurement can be made, is provided in the next section.

5 Sensitivity Analysis

As previously described, the system may take on two distinct forms: (1) one that utilizes a coherent detection scheme (CDS), and (2) another that uses a pump-probe scheme (PPS). The goal of both systems is an accurate and a very sensitive determination of the BGS, from which can be derived the distribution of a fiber's environment. Both methods require the use of a narrow linewidth spectrally tunable source. For the CDS, this is the local oscillator (LO) and for the PPS this becomes the probe wavelength. The LGF possesses a Brillouin frequency that is lengthwise distributed and monotonic in its change. In principle, this means that each unique frequency component of the Brillouin spectrum maps exactly to a single point on the fiber. As such, the spectral width ($\Delta\nu_L$) of the laser of which frequency is swept through the BGS, therefore represents the absolute limiting spatial resolution for the frequency-domain system based on a LGF. Here, resolution is the uncertainty in the position determined for a single event. This limiting spatial resolution (Δl) can be written in terms of the sensor (fiber) length, L, and total breadth of frequency, B_S, possessed by the BGS of the fiber (for a linear frequency distribution) as

$$\Delta l = \frac{\Delta\nu_L}{B_S} L. \tag{6}$$

For example, assuming a fiber length of 1 km, a Brillouin spectral breadth of 1 GHz along that fiber length, laser linewidths of 1 MHz and 100 kHz give rise to absolute minimum spatial resolutions of 1 m and 10 cm, respectively. Alternatively, for a fiber with a length of 10 m and all other parameters kept the same, the minimum spatial resolutions become 1 cm and 1 mm, respectively. Since the fiber may be designed to be application specific, LGFs are not necessarily limited to long-[11] or short-range[25] applications.

While the un-chirped spectral width of an optical fiber may be on the order of a few tens of MHz, even a small change in temperature results in a measurable and calculable change in the BGS. However, the ability to measure these small changes in the BGS is limited by system noise. From them, it is possible to estimate the measurement (temperature or strain) resolution of a LGF-based system. In the following subsections, the noise sources relevant to each system are identified and listed, and noise variances (in units of Amperes squared, A^2) and SNRs are calculated and presented. The noise variances are converted into a measurement resolution in the following way: a total noise variance σ^2_{total} is calculated with the standard deviation clearly setting the minimum detectable change in the BGS, as outlined in Fig. 9. The BGS is calculated for decreasing temperature or strain, and the point where $\Delta A/2$ (ΔA is the magnitude of change in the BGS from the unperturbed stated, as illustrated in Fig. 9) falls to σ_{total} is considered to be the measurement limit.

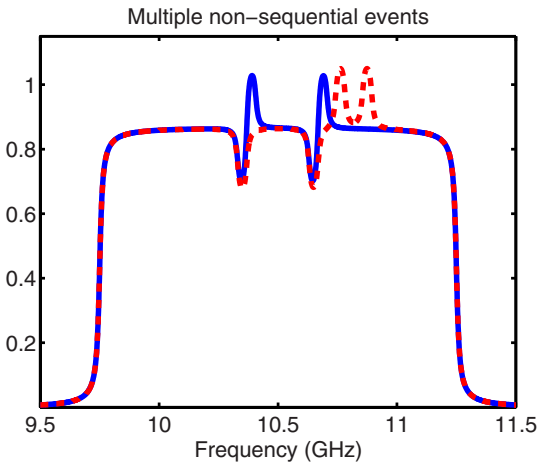

Fig. 8 An example of a possible nonsequential BGS. It is clear from the spectrum that at least two events (local heating or strain) have taken place, but it is not readily apparent which of the two peaks (dashed line) corresponds to which location along the fiber. Tracking the BGS in time can alleviate this problem.

5.1 *Coherent Detection Scheme*

An example of a possible CDS arrangement is shown in Fig. 10. The pump signal passes through an optical circulator and into the sensor fiber through a second port. The generated Brillouin signal is backscattered and passes through the third port of the circulator to an optical amplifier that may possess a bandpass optical filter. This signal is then combined with a tunable local oscillator signal onto a receiver,

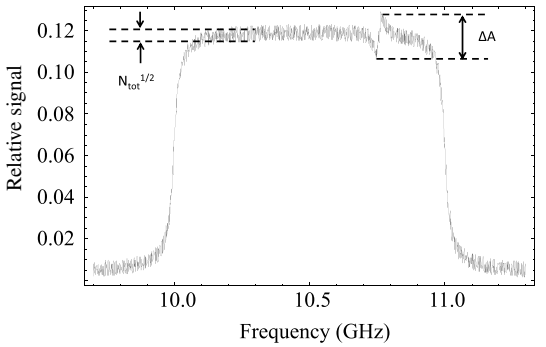

Fig. 9 Simulated noisy BGS measurement illustrating the standard deviation of the noise and ΔA. Noises are assumed to be Gaussian distributed.

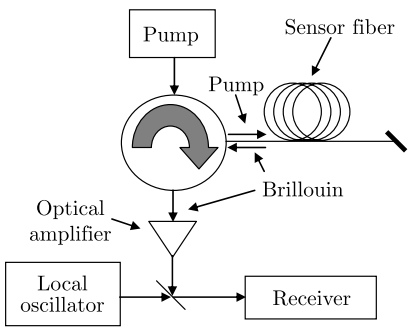

Fig. 10 Example of a CDS configuration.

with the resulting generated electrical signal being processed via electronics and software (not shown).

Two electric field components are present at the detector. These are the LO and Brillouin (designated as "S") signals:

$$E_{\mathrm{LO}} \propto \sqrt{P_{\mathrm{LO}}} e^{-j\omega_{\mathrm{LO}}(t)t}, \tag{7}$$

$$E_S \propto \sqrt{P_S} e^{-j\omega_S(z)t}. \tag{8}$$

In Eqs. (7) and (8), P is the optical power. The time or lengthwise dependencies of the angular frequencies, ω, reflect the nature of the signals produced, that is, the local oscillator frequency will be swept, while the SBS signal has a frequency distribution that is fiber dependent. The determination of $|E_{\mathrm{LO}} + E_S|^2$ and the assumption of a detector responsivity, $\mathbf{R}$ (A/W), gives rise to the following current signal that is produced by the system

$$i_{\mathrm{sig}} = \mathbf{R}\left(P_{\mathrm{LO}} + P_S + 2\sqrt{P_{\mathrm{LO}}P_S}\cos\{[\omega_{LO}(t) - \omega_S(t)]t\}\right). \tag{9}$$

In Eq. (9), although P_s may not be polarized identically with P_{LO}, it is assumed in the subsequent analysis that the polarization components can be treated independently (optically polarization split) and that the resulting electrical signals are added after the electrical mixing.[43] This is considered to be a reasonable first-order approximation given in the exploratory nature of this sensitivity analysis. In a homodyne system, a change in the direct current level is detected as $\omega_{\mathrm{LO}}(t)$ is swept through $\omega_{\mathrm{SBS}}(z)$ or when $\omega_{\mathrm{LO}}(t) = \omega_S(z_1)$. Thus, the relevant detected homodyne signal, then, is $2\mathbf{R}\sqrt{P_{\mathrm{LO}}P_S}$.

Next, the noise variances (units of A^2) are identified and listed. The thermal noise is given by

$$\sigma_T^2 = \frac{4kTB_N}{R}, \tag{10}$$

where k is Boltzmann's constant (1.38×10^{-23} J/K), T is the absolute temperature (K), R is a noise equivalent receiver resistance (Ohms), and B_N is the bandwidth of the receiver system (Hz). In the present system, since a BGS sweep may be 1 s or longer, the thermal and other noises can be considerably reduced if the receiver bandwidth is limited to less than about 10 kHz. Shot noise is contributed to by the presence of the LO and SBS signals, while the former usually is much larger than the latter. The SBS signal is the total integrated SBS power in the received signal (over the entire BGS). $P_{S,\mathrm{total}}$ is distinct from P_S in that the latter is the integrated SBS power over the LO spectrum. Shot noise, then, is given by

$$\sigma_{\mathrm{Shot}}^2 = 2e\mathbf{R}(P_{\mathrm{LO}} + P_{S,\mathrm{total}})B_N \approx 2e\mathbf{R}P_{\mathrm{LO}}B_N, \tag{11}$$

where e is the electron charge (1.6×10^{-19} C). Other dominant noises include beat noises associated with the various optical signal components that are present. First, in a system that is optically amplified (as is the case with the CDS), amplified spontaneous emission (ASE) can beat with the LO and SBS signals and with itself. The noise variances are[44–46]

$$\sigma_{\mathrm{ASE-ASE}}^2 = 4N_{\mathrm{ASE}}^2 B_o B_N \mathbf{R}^2, \tag{12}$$

$$\sigma_{S-\mathrm{ASE}}^2 = 4N_{\mathrm{ASE}}(P_{\mathrm{LO}} + P_{S,\mathrm{total}})B_N\mathbf{R}^2 \approx 4N_{\mathrm{ASE}}P_{\mathrm{LO}}B_N\mathbf{R}^2, \tag{13}$$

where $B_O (\gg B_N)$ is the optical bandwidth of the ASE noise spectrum, N_{ASE} (W/Hz), which is assumed to be optically filtered with a passband of B_o. Similarly, since there is also Brillouin spontaneous scattering, these beat noises may be presented as well. Similar to Eqs. (12) and (13), including an ASE–SBS term, these can be described as

$$\sigma_{\mathrm{SBS-SBS}}^2 = 4N_S^2 B_S B_N \mathbf{R}^2, \tag{14}$$

$$\sigma_{\mathrm{LO-SBS}}^2 = 4N_S P_{LO} B_N \mathbf{R}^2, \tag{15}$$

$$\sigma_{\mathrm{ASE-SBS}}^2 = 4N_S N_{\mathrm{ASE}} B_S B_N \mathbf{R}^2, \tag{16}$$

where N_S is the spectral power density (W/Hz) of the generated Brillouin signal, and B_S is the spectral breadth of the fiber BGS (units of Hz).

For a uniformly distributed BGS, the Brillouin signal power is related to the power density and LO laser linewidth as $P_S = N_S\Delta\nu_L$. In Eq. (16), it is assumed that, most typically, $B_S \ll B_O$. Seven noise sources have been identified, and other possible noise sources (such as laser relative intensity noise) can be rendered negligible through careful selection of system components.

In order to calculate $P_S(=\Delta\nu_S N_S)$, the analysis found in Boyd et al.[47] was utilized where a Brillouin reflectivity, R_B, was used to determine the total Brillouin signal density, $N_S(N_S = PR_B/B_S)$ appearing at the receiver,

$$R_B = Ye^{G'/2}\left[I_0\left(\frac{G'}{2}\right) - I_1\left(\frac{G'}{2}\right)\right], \tag{17}$$

where I_m is the modified Bessel function of order m and

$$Y = (\bar{n}+1)g_B h\nu_S \Gamma \frac{L}{4A}, \tag{18}$$

$$G' = g_B \frac{P}{A}L, \tag{19}$$

$$\bar{n} = \left[\exp\left(\frac{h\nu_B}{kT}\right) - 1\right]^{-1}, \tag{20}$$

and where P is the pump power launched into the fiber, A is the mode effective area (determined from the MFD), ν_S is the frequency of the Stokes' signal (approximately equal to that of the pump signal), and Γ is the decay rate ($\Gamma = \pi B_S$).The Brillouin frequency ν_B was arbitrarily selected for convenience to be 11 GHz, and the remaining assumed values can be found in Table 1. Since N_S is small, it is anticipated that the optical preamplification will be applied via an EDFA and an optical power gain, G, of 30 dB is assumed available. Thus, in each of the relevant noise equations, the fiber-amplified value GN_S is utilized. Finally, the total SNR of the system can be calculated using

$$\mathrm{SNR} = \frac{2\mathbf{R}\sqrt{P_{\mathrm{LO}}P_S}}{\sqrt{\sum_{m=1}^{7}\sigma_m^2}}, \tag{21}$$

where the summation is over the identified noise variances [Eqs. (10)–(16)].

Next, an example is presented to determine the relative strengths of each of these sources of noise. Table 1 lists the assumptions made for the example of a distributed temperature sensor. The optical bandwidth B_O is assumed to be conditioned by a bandpass filter, such as a Bragg grating assembly, and the SBS bandwidth B_S is assumed to be limited by the spectral extent of the fiber BGS, in this case, assumed to be 1 GHz linearly distributed over a fiber length, L, of 1000 m, such that the BGS is approximately uniform in shape.

Figures 11 and 12 display the logarithm of the calculated noise variance for each identified source (for $B_N = 1$ kHz) and the SNRs versus P for several B_N, respectively. Both the thermal and shot noises are dominated by the other noises and can be neglected here. Inspection of Fig. 12 shows that there is a range of optimal P's where the SNR is maximized. This can be explained as follows. As the power increases, SNR increases as expected. However, since the second dominant noise source [SBS–SBS Eq. (14)] is dependent on N_S^2 and P_S on N_S, at very large values of P, the SNR will begin to decrease as the inverse of $N_S^{1/2}$.

In order to estimate the sensitivity or thermal resolution in the context of the previous set of calculations, the method outlined in the beginning of this section is utilized. Strain is considered in the next paragraph. Assuming the resolution limit for the present case ($\Delta\nu_L L/B_S = 1$ m) and an SNR of around 100 (100 Hz B_N case), a temperature resolution of about 10 K is obtained. While at first glance this may not seem very impressive, this system resolution is for a single BGS sweep that can be performed as quickly as 10 ms due to B_N (and limited by the electronics and laser tuning speed). As such, if a measurement integration can be done such that the measurement of a thermal distribution is averaged over several seconds, the noises can be greatly diminished, and a

Table 1 Values assumed for the example calculation presented here.

Parameter	Symbol	Value assumed	Unit
Local oscillator power	P_{LO}	1	mW
Detector responsivity	**R**	1	A/W
System electrical bandwidth	B_N	0.1, 1, 10	kHz
System temperature	T	300	K
Noise equivalent resistance	R	1	kΩ
Center optical wavelength	λ_O	1550	nm
Optical passbandwidth	B_O	0.1	nm
Optical passbandwidth	B_O	12.5	GHz
Total Brillouin spectral width of the LGF	B_S	1	GHz
Sensor length	L	1000	M
LO or probe laser spectral width	$\Delta\nu_L$	1	MHz
Brillouin frequency shift	ν_B	11	GHz
Mode field diameter	MFD	10	μm
Fiber amplifier gain	G	30	dB
Spontaneous emission noise power spectral density	N_{ASE}	10^{-15}	W/Hz
Brillouin gain coefficient	g_B	0.12×10^{-11}	m/W
Brillouin shift temperature coefficient	C_T	1.11	MHz/K
Brillouin shift strain coefficient	C_ε	500	MHz/%

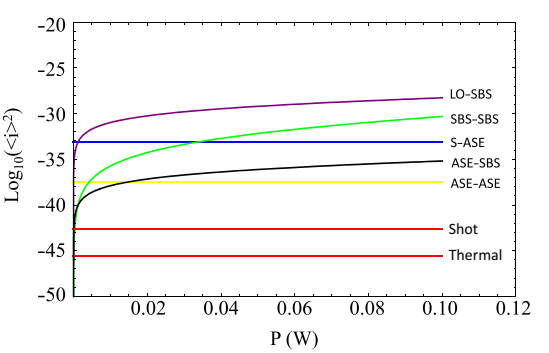

Fig. 11 Logarithm of the variances of the various identified noise sources.

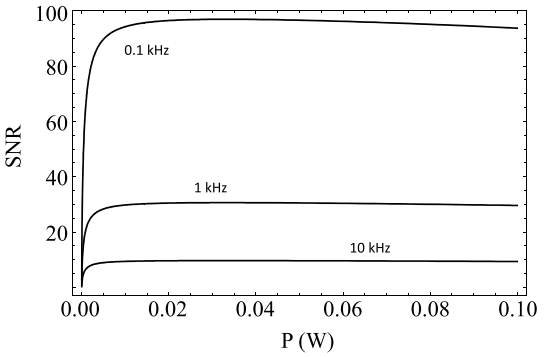

Fig. 12 SNR of the homodyne system plotted as a function of P for three different electrical bandwidths B_N.

considerable improvement in the sensitivity can be achieved. This, of course, will depend on system requirements, and therefore a detailed analysis is not provided here. As it stands, a single-sweep system could be implemented as a rapid-detection thermal alarm system for a structure.

Finally, this subsection is concluded with a discussion of the strain. In principle, the measurement of strain rather than temperature is entirely feasible, and the entirety of the above noise analysis holds for that case. However, in the sensitivity analysis, the assumption is made that the Brillouin frequency shift increases at a rate of about 500 MHz/% of strain. Thus, recalculating the strain sensitivity using the identical set of assumptions provided above, a minimum detectable applied strain is found to be about 0.02%. Again, this is the sensitivity in the lengthwise resolution limit in a single measurement sweep.

5.2 *Pump-Probe Scheme*

An example of a possible PPS arrangement is shown in Fig. 13. The pump signal passes through an optical circulator and into the sensor fiber through a second port. A probe signal is launched into the far end of the sensor fiber and experiences gain due to SBS in the sensor fiber. The Brillouin-amplified probe signal then passes through the third port of the circulator and into a receiver. The resulting generated electrical signal is processed via electronics and software (not shown).

In the case of the PPS, the measured signal is that of an amplified probe source that backpropagates through the sensor fiber in a direction opposite to that of the pump. Gain originates from SBS itself, and thus the need for optical amplification generally is deemed unnecessary. The amplified probe power at the receiver can be expressed as a

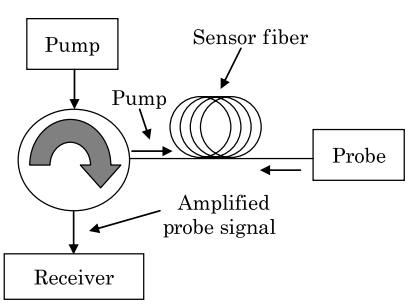

Fig. 13 Example PPS configuration.

function of the Brillouin gain provided in Eq. (19) and the input probe power (P_{probe}) as $P_S' = P_{\text{probe}} e^{G'}$. From a system perspective, an unamplified probe signal (outside of the Brillouin gain band) leads to an offset in the measured signal, much like a nonzero space (a zero in a binary system) in a lightwave communications system. As a result, meaningful information in the measured Brillouin-amplified signal is therefore the change in power, which gives rise to an electrical signal (current) having the form

$$i_{\text{sig}} = \mathbf{R} P_{\text{probe}} (e^{G'} - 1). \tag{21}$$

Since an optical amplifier is not used, all but Eqs. (12), (13), and (16) remain relevant to the PPS configuration. In moving to the PPS from the CDS, Eqs. (10) and (14) remain the same, while the optical power terms in Eqs. (11) and (15) are replaced by P_S' [i.e., $P_{\text{LO}} + P_S \rightarrow P_S'$ and $P_{\text{LO}} \rightarrow P_S'$ in Eqs. (11) and (15), respectively] since P_S' represents the total optical power at the receiver. The assumption is made that the Brillouin spontaneous scattering signal is unchanged with changes in the probe power (i.e., un-depleted pump approximation), which is reasonable at low probe power.

Utilizing a pump power of 100 mW, Figs. 11 and 12 are repeated for the PPS configuration as a function of probe power and are provided as Figs. 14 and 15 utilizing $B_N = 1$ kHz and identically all relevant quantities found in Table 1. From the figures, it is clear that, at least in terms of the SNR ($= i_{\text{sig}}/\sqrt{\sum_{m=1}^{4} \sigma_m^2}$), the PPS is vastly superior to the CDS. This can be understood by considering that (1) the signal power in the PPS scheme is much larger than in the CDS scheme, (2) the spontaneous Brillouin scattering noise is not preamplified before entering the receiver, and (3) the gain term in Eq. (22) prevents the Brillouin spontaneous scattering noise from dominating the system at any pump power. The advantage of the CDS, however, over the PPS is that it is a true reflectometry system, whereas the PPS requires either a probe laser at the far end of the sensor fiber or some type of reflector (such as a coated end-facet or fiber Bragg grating) at the far end of the sensor fiber or a second fiber and loop through which one launches the probe signal. Any of these possibilities may be infeasible depending on the system or environment.

The SNRs utilizing other electrical filter bandwidths were not calculated due to the already large values. Using the results in Fig. 15, and assuming an SNR above 10^3 can be achieved, the sensitivity of the system can be estimated

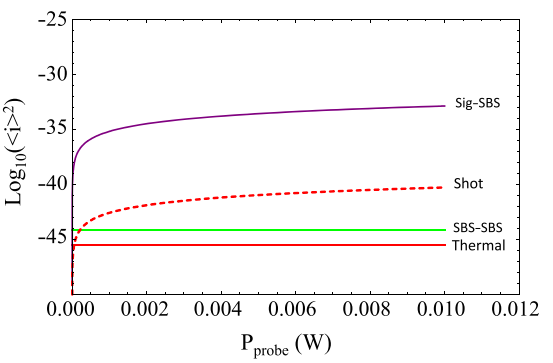

Fig. 14 Logarithm of the variances of the various identified noise sources for the PPS configuration. The variance is calculated in units of Amperes squared.

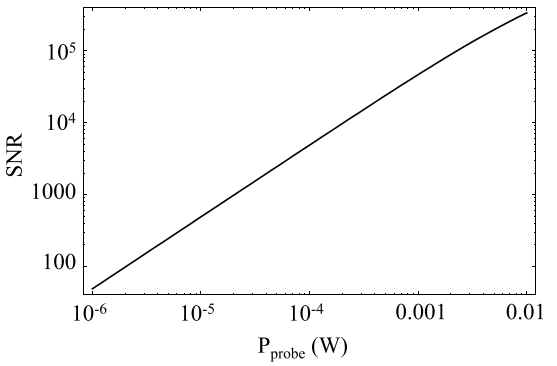

Fig. 15 SNR of the pump-probe system plotted as a function of probe power for $B_N = 1$ kHz.

utilizing the same method as above, giving rise to one that is below 0.5 K in a single frequency sweep of the probe laser. The lengthwise absolute resolution of the system in this case remains 1 m, as with the CDS example, limited by the probe laser spectral width. This suggests a highly sensitive and rapid measurement system is possible in the frequency domain utilizing LGF in a chirped fiber sensor configuration.

6 Conclusion

A new type of frequency domain, Brillouin-based distributed sensing system was proposed, outlined, and evaluated. The system utilizes a LGF, of which Brillouin frequency changes with position along the fiber, which then is an intrinsically "chirped fiber." Since each frequency on the Brillouin spectrum maps one-to-one to a position along the fiber, a change in the Brillouin spectrum at some frequency represents an environmental event at the same position along the fiber. As such, the distributions of temperature or strain will result in a measureable change in the whole BGS. Experimental measurements on an LGF with roughly 100 MHz acoustic frequency chirped distributed over 16.7 m demonstrated the potential of such a frequency-domain system. Uniformly heated were 1.1 and 1.7 m segments of this LGF, through which a model was shown to extremely well predict the measured BGS, rendering the BGS calculable for a known temperature/strain distribution. The segments were uniformly heated up to 40 K above ambient.

In a system, with knowledge of the unperturbed spectrum, the perturbed fiber spectrum gives rise to a lengthwise measurement of the temperature or strain. Since the system requires CW lasers and a BGS is measured in order to determine $T(z)$ and $\varepsilon(z)$, this can be classified as a frequency-domain distributed sensing system. Sensitivity analyses based on coherent detection and PPS were performed and showed that these systems have the potential to achieve very high SNR values with sub-1 K and sub-meter measurement accuracy in a single, extremely rapid scan of the BGS. Pump-probe methods seem to have a considerable advantage over their coherent counterparts.

The mathematical analysis presented here was limited to the case of distributed sensing of events that may trigger an alarm, such as a fire, intrusion, or leak. High spatial resolution with the ability to resolve two closely spaced simultaneous events will require LGFs with greater total frequency span, or larger values of C (MHz/m). Furthermore, measurements were limited due to the relatively short available length of proof-of-concept fiber. As such, work is currently underway to increase the length of fibers and expanding the total breadth of the Brillouin spectrum, and results are forthcoming.

Acknowledgments

The authors wish to thank A. Evert and T. Hawkins (Clemson University) for fabricating the LGF utilized in this study and Dr. R. Rice (Dreamcatchers Consulting) for fruitful discussions and encouragement. A. Mangognia is supported by the Joint Technology Office through Contract No. W911NF-12-1-0602.

References

1. W. A. Goodman, "Athermal glass by design," *Proc. SPIE* **6666**, 666604 (2007).
2. Y. Himei et al., "Transparent athermal glass-ceramics in Li_2O-Al_2O_3-SiO_2 system," *Proc. SPIE* **5723**, 71–78 (2005).
3. M. Guignard, L. Albrecht, and J. W. Zwanziger, "Zero-stress optic glass without lead," *Chem. Mater.* **19**, 286–290 (2007).
4. T. Fukazawa, M. Korekawa, and Y. Fujita, "Spectroscopic photoelasticity of lead-silica glass analyzed by polarization modulated ellipsometry," *J. Non-Cryst. Solids* **203**, 102–108 (1996).
5. M. Niklès, L. Thévenaz, and P. A. Robert, "Brillouingain spectrum characterization in single-mode optical fibers," *J. Lightwave Technol.* **15**, 1842–1852 (1997).
6. P.-C. Law et al., "Acoustic coefficients of P_2O_5-doped silica fiber: acoustic velocity, acoustic attenuation, and thermo-acoustic coefficient," *Opt. Express* **1**, 686–699 (2011).
7. P.-C. Law, A. Croteau, and P. D. Dragic, "Acoustic coefficients of P_2O_5-doped silica fiber: the strain-optic and strain-acoustic coefficients," *Opt. Express* **2**, 391–404 (2012).
8. D. Culverhouse et al., "Potential of stimulated Brillouin scattering as a sensing mechanism for distributed temperature sensors," *Electon. Lett.* **25**, 913–914 (1989).
9. T. Kurashima, T. Horiguchi, and M. Tateda, "Distributed-temperature sensing using stimulated Brillouin scattering in optical silica fibers," *Opt. Lett.* **15**, 1038–1040 (1990).
10. T. Kurashima, T. Horiguchi, and M. Tateda, "Tensile strain dependence of Brillouin frequency shift in silica optical fibers," *IEEE Phot. Technol. Lett.* **1**, 107–109 (1989).
11. X. Bao, D. J. Webb, and D. A. Jackson, "22 km distributed strain sensor using Brillouin loss in an optical fibre," *Opt. Commun.* **104**, 298–302 (1994).
12. A. Minardo, L. Zeni, and R. Bernini, "High-spatial- and spectral-resolution time-domain Brillouin distributed sensing by use of two frequency-shifted optical beam pairs," *IEEE Photon. J.* **4**, 1900–1908 (2012).
13. R. K. Yamashita et al., "Measurement range elongation based on temporal gating in Brillouin optical correlation domain distributed simultaneous sensing of strain and temperature," *IEEE Photon. Technol. Lett.* **24**, 1106–1108 (2012).
14. Y. Peled, A. Motil, and M. Tur, "Fast Brillouin optical time domain analysis for dynamic sensing," *Opt. Express* **20**, 8584–8591 (2012).
15. Y. Dong et al., "2 cm spatial-resolution and 2 km range Brillouin optical fiber sensor using a transient differential pulse pair," *Appl. Opt.* **51**, 1229–1235 (2012).
16. R. Bernini, A. Minardo, and L. Zeni, "Dynamic strain measurement in optical fibers by stimulated Brillouin scattering," *Opt. Lett.* **34**, 2613–2615 (2009).
17. C.A. Galindez et al., "30 cm of spatial resolution using pre-excitation pulse BOTDA technique," *Proc. SPIE* **7753**, 77532H (2011).
18. Y. Mao et al., "1-cm-spatial-resolution Brillouin optical time-domain analysis based on bright pulse Brillouin gain and complementary code," *IEEE Photon. J.* **4**, 2243–2248 (2012).
19. Y. Mizuno, Z. He, and K. Hotate, "One-end-access high-speed distributed strain measurement with 13-mm spatial resolution based on Brillouin optical correlation-domain reflectometry," *IEEE Phot. Technol. Lett.* **21**, 474–476 (2009).
20. A. W. Brown, B. G. Colpitts, and K. Brown, "Dark-pulse Brillouin optical time-domain sensor with 20-mm spatial resolution," *J. Lighwave Technol.* **25**, 381–386 (2007).
21. X. Bao and L. Chen, "Recent progress in Brillouin scattering based fiber sensors," *Sensors* **11**, 4152–4187 (2011).
22. C. A. Galindex-Jamioy and J. M. López-Higuera, "Brillouin distributed fiber sensors: an overview and applications," *J. Sensors* **2012**, 204121 (2012).
23. Z. Liu et al., "Brillouinscattering based distributed fiber optic temperature sensing for fire detection," *Fire Safety Sci.* **7**, 221–232 (2003).
24. S. Grosswig et al., "Pipeline leakage detection using distributed fibre optical temperature sensing," *Proc. SPIE* **5855**, 226–229 (2005).

25. V. P. Ranendran et al., "Use of fiber optic based distributed temperature measurement system for electrical machines," *Proc. SPIE* **5191**, 214–225 (2003).
26. P. Ferdinand et al., "Brillouin sensing for perimetric detection: the SmartFence project," *Proc. SPIE* **8421**, 84219X (2012).
27. H. Ohno et al., "Industrial applications of the BOTDR optical fiber strain sensor," *Opt. Fib. Technol.* **7**, 45–64 (2001).
28. D. Garus et al., "Distributed sensing technique based on Brillouin optical-fiber frequency-domain analysis," *Opt. Lett.* **21**, 1402–1404 (1996).
29. R. Bernini, "Centimeter-range spatial resolution distributed sensing by BOFDA," *Proc. SPIE* **7753**, 77532C (2011).
30. A. K. Sang et al., "Millimeter resolution distributed dynamic strain measurements using optical frequency domain reflectometry," *Proc. SPIE* **7753**, 77532S (2011).
31. G.C. Papen, W.M. Pfenninger, and D.M. Simonich, "Sensitivity analysis of Na narrowband wind-temperature lidar systems," *Appl. Opt.* **34**, 480–498 (1995).
32. R. L. Schwiesow and L. Lading, "Temperature profiling by Rayleigh-scattering lidar," *Appl. Opt.* **20**, 1972–1979 (1981).
33. C. G. Carlson et al., "High power Yb-doped fiber laser-based LIDAR for space weather," *Proc. SPIE* **6873**, 68730K (2008).
34. W. Zou et al., "Stimulated Brillouin scattering and its dependences on strain and temperature in a high-delta optical fiber with F-doped depressed inner cladding," *Opt. Lett.* **32**, 600–602 (2007).
35. P. D. Dragic, "Novel dual-Brillouin-frequency optical fiber for distributed temperature sensing," *Proc. SPIE* **7197**, 719710 (2009).
36. P. Dragic et al., "Sapphire-derived all-glass optical fibres," *Nat. Photon.* **6**, 627–633 (2012).
37. Y. Mizuno and K. Nakamura, "Potential of Brillouin scattering in polymer optical fiber for strain-insensitive high-accuracy temperature sensing," *Proc. SPIE* **7753**, 775329 (2011).
38. A. Evert et al., "Longitudinally-graded optical fibers," *Opt. Express* **20**, 17393–17402 (2012).
39. P. D. Dragic, "Simplified model for effect of Ge doping on silica fibre acoustic properties," *Electron. Lett.* **45**, 256–257 (2009).
40. B. Ward and J. Spring, "Finite element analysis of Brillouin gain in SBS-suppressing optical fibers with non-uniform acoustic velocity profiles," *Opt. Express* **17**, 15685–15699 (2009).
41. A. Safaai-Jazi and R. O. Claus, "Acoustic modes in optical fiberlike waveguides," *IEEE Trans. Ultrason. Ferroelec. Freq. Control.* **35**, 619–627 (1988).
42. P. D. Dragic, "Estimating the effect of Ge doping on the acoustic damping coefficient via a highly Ge-doped MCVD silica fiber," *J. Opt. Soc. Am. B.* **26**, 1614–1620 (2009).
43. M. Kavehrad and B. S. Glance, "Polarization-insensitive frequency shift keying optical heterodyne receiver using discriminator demodulation," *J. Lightwave Technol.* **6**, 1386–1394 (1988).
44. A. Yariv, "Signal-to-noise considerations in fiber links with periodic or distributed optical amplification," *Opt. Lett.* **15**, 1064–1066 (1990).
45. S. Donati and G. Giuliani, "Noise in an optical amplifier: formulation of a new semiclassical model," *J. Quantum Electron.* **33**, 1481–1487 (1997).
46. J. L. Rebola and A.V. T. Cartaxo, "Q-factor estimation and impact of spontaneous-spontaneous beat noise on the performance of optically preamplified systems with arbitrary optical filtering," *J. Lightwave Technol.* **21**, 87–95 (2003).
47. R.W. Boyd, K. Rzażewski, and P. Narum, "Noise initiation of stimulated Brillouin scattering," *Phys. Rev. A.* **42**, 5514–5521 (1990).

Peter D. Dragic received his PhD degree in 1999 from the University of Illinois, Urbana-Champaign (UIUC). His interests include next-generation laser sources and optical fiber for remote-sensing applications. Part of this emphasis is on the mitigation of nonlinear optical fiber phenomena that limit scalability in these systems. He has been involved with the launch of several start-up companies and is currently a lecturer in the department of electrical and computer engineering at UIUC.

Anthony Mangognia is a PhD degree candidate in the Department of Electrical and Computer Engineering at the University of Illinois, Urbana-Champaign, where he also received his BS and MS degrees in electrical engineering. His primary research area is remote sensing and space physics, with a focus on laser remote sensing. He has been involved with the development of the Andes LiDAR observatory. His interests include fiber lasers and amplifiers, cubesat technology, and optical fiber SBS characterization.

John Ballato is a professor of materials science and engineering at Clemson University, South Carolina. He has published 300 archival scientific papers, holds over 25 U.S. and foreign patents, and has given in excess of 150 keynote/invited lectures, and has co-organized 70 national and international conferences and symposia. Among numerous other honors, he is a fellow of the Optical Society of America (OSA), SPIE, and the American Ceramic Society (ACerS).